Proceedings of the International School-seminar
"New Physics and Quantum Chromodynamics at External Conditions", pp. 49 – 56,
May 22-24, 2013, Dnipropetrovsk, Ukraine

NEUTRINO MAGNETIC MOMENT AS A SIGNAL OF NEW PHYSICS

O.M.Boyarkin [a], G.G.Boyarkina [b]

Belarus State Pedagogical University, Minsk, Belarus

Within the left-right model with Majorana neutrinos the corrections to neutrino dipole magnetic moments (DMM) coming from the $\tilde{\delta}^{(\pm)}$-Higgs bosons are considered. It is shown that when $\tilde{\delta}^{(\pm)}$-bosons are on the electroweak scale then their contributions to the DMM are comparable with, and even could exceed, the contributions of the charged gauge bosons. The behavior of a neutrino flux in matter and a magnetic field is investigated. It was proven that even at $E_\nu > m_N$ the resonance transitions between the light and heavy neutrinos are forbidden. Investigation of the collider experiments with the light neutrino beam revealed that we can detect both the μ^{NN} and $\mu^{\nu N}$ moments. The most perspective reactions are

$$\nu_{\mu L} + p \to N_{\mu R} + X, \qquad p + p \to \gamma^* \to N_{eR} + \overline{\nu}_{eL} + X, \qquad p + p \to W_R^* \to e + N_e \to e + \nu_e + \gamma + X.$$

1 Introduction

At the end of 2002 as consequence of series of experiments with solar, atmospheric and reactor neutrinos the existence of the neutrino oscillations has been established. This, in turn, meant that the neutrino has a mass and the partial lepton flavor violation takes place. At the same time monitoring of the Galaxy by the net of neutrino telescopes aimed to detect a neutrino signal from the expected galactic supernova explosion has been starting. Neutrinos also find a use for solution of applied problems as evidenced by the application of antineutrino detectors for nuclear reactor monitoring in the "on-line" regime and the appearance of a neutrino geotomography (see, for review, [1]). All this puts forward the neutrino physics in the forefront of natural sciences. However, in spite of achieved progress there are series unsolved problems in the neutrino physics. Among these first of all are: (i) the smallness of the neutrino mass $m_\nu \approx 10^{-6} m_e$; (ii) the value of the neutrino dipole magnetic moment (DMM); (iii) the neutrino nature (Dirac or Majorana).

Models with the see-saw mechanism give successful explanation of the first problem. In these models heavy right-handed neutrinos being see-saw partners of light left-handed neutrinos appear. Introducing of heavy neutrinos N_i $(i = 1, 2, 3)$ helps to solve some cosmological problems as well. For example, these neutrinos are used for explanation of the observed baryon asymmetry in the Universe thanks to the leptogenesis.

Interest in electromagnetic neutrino properties is primarily caused by the fact that there exist plenty of astrophysical systems with intensive magnetic fields where neutrino physics plays an important part. Large magnetic fields are present in supernovas, neutron stars and white dwarfs, and fields as large as $B_e = m_e^2/e \simeq 4.41 \times 10^{13}$ G can arise in supernova explosions or coalescing neutron stars.

In the standard model (SM) neutrinos are massless particles and the mixing of neutrino states do not take place. Reconstruction of the neutrino sector of the SM is usually achieved by introducing a right-handed neutrino singlet (minimally extended SM). However, the explanation of the neutrino mass smallness is absent. DMM's predicted by the SM are so small that they are not of any physical interest. It should be also noted that in the SM the satisfactory mechanism to produce a baryonic asymmetry in the universe is absent. All this taken together provides strong evidence of Physics beyond the SM.

The purpose of our work is investigation of the neutrino electromagnetic properties in the context of the left-right-symmetric model (LRM).

2 The left-right-symmetric model

For the first time the model based on the $SU(2)_L \times SU(2)_R \times U(1)_{B-L}$ gauge group (LRM) was proposed at the beginning of the 1970s [2]. In the LRM quarks and leptons enter into the left- and right-handed doublets

$$Q_L^a(\frac{1}{2}, 0, \frac{1}{3}) = \begin{pmatrix} u_L^a \\ d_L^a \end{pmatrix}, \qquad Q_R^a(0, \frac{1}{2}, \frac{1}{3}) = \begin{pmatrix} u_R^a \\ d_R^a \end{pmatrix},$$

e-mail: [a]oboyarkin@tut.by, [b]boyarkin@front.ru

$$\Psi^a_L(\frac{1}{2},0,-1)=\begin{pmatrix}\nu_{aL}\\ l_{\alpha L}\end{pmatrix},\qquad \Psi^a_R(0,\frac{1}{2},-1)=\begin{pmatrix}N_{aR}\\ l_{aR}\end{pmatrix}. \tag{1}$$

where $a=1,2,3$, in brackets the values of S^W_L, S^W_R and $B-L$ are given, S^W_L (S^W_R) is the weak left (right) isospin while B and L are the baryon and lepton numbers. The gauge boson sector include four charged bosons ($W^{\pm}_L$, $W^{\pm}_R$) and two neutral bosons (Z_L and Z_R). There are two possibilities of defining the LR symmetry as a generalized parity P and as a generalized charge conjugation C. It was found that $m_{W_2}>2.5$ TeV if LR=C and $m_{W_2}>4$ TeV if LR=P. We remind that there is the theoretical relation $m_{Z_R}\approx 1.7 m_{W_R}$ too.

The Higgs sector structure determines the neutrino nature. The mandatory element of the Higgs sector is the bi-doublet $\Phi(1/2,1/2,0)$. For the neutrino to be a Majorana particle, the Higgs sector must include two triplets $\Delta_L(1,0,2)$, $\Delta_R(0,1,2)$.

The SSB according to the chain

$$SU(2)_L\times SU(2)_R\times U(1)_{B-L}\to SU(2)_L\times U(1)_Y\to U(1)_Q$$

is realized for the following choice of the VEVs:

$$<\delta^0_{L,R}>=\frac{v_{L,R}}{\sqrt{2}},\qquad <\Phi^0_1>=k_1,\qquad <\Phi^0_2>=k_2, \tag{2}$$

$$v_L<<\max(k_1,k_2)<<v_R. \tag{3}$$

After the SSB we are left with 14 physical Higgs bosons: four doubly-charged scalars $\Delta^{(\pm)}_{1,2}$, four singly-charged scalars $\delta^{\tilde{(\pm)}}$ and $h^{(\pm)}$, four neutral scalars $S_{1,2,3,4}$, and two neutral pseudoscalars $P_{1,2}$. The detailed discussion of the Higgs sector structure has been done in [3].

It could be shown that the $\delta^{\tilde{(\pm)}}$-boson whose mass is defined as

$$m^2_{\tilde{\delta}}=(\rho_3/2-\rho_1)v^2_R-\frac{\beta^2k^2_0}{\alpha+\rho_1-\rho_3/2}, \tag{4}$$

where

$$k_{\pm}=\sqrt{k^2_1\pm k^2_2},\qquad k_0=\frac{k^2_-}{\sqrt{2}k_+},\qquad \alpha=\frac{\alpha_3k^2_+}{2k^2_-},\qquad \beta=\frac{k^2_+(\beta_1k_1+2\beta_3k_2)}{2k^2_-k_0}, \tag{5}$$

$k_+=174$ GeV, and $\beta_1,\beta_3,\alpha_3,\rho_1,\ \rho_3$ are the constants entering into the Higgs potential, may lie on the electroweak scale (EWS). It is possible under conditions

$$\alpha\approx 1,\qquad (\rho_3/2-\rho_1)\approx\frac{k^2_+ +3\beta^2k^2_0}{3v^2_R}. \tag{6}$$

Note, when this scenario is realized two physical Higgs bosons S_4 and P_2 whose masses are

$$m^2_{S_4}=(\rho_3/2-\rho_1)v^2_R,\qquad m^2_{P_2}=(\rho_3/2-\rho_1)v^2_R \tag{7}$$

lie on the EWS too.

For a massive Dirac neutrino the most general form of the matrix element for the conserved neutrino electromagnetic current J^{em}_μ is given by the expression

$$<\nu^D_i(p')|J^{em}_\mu|\nu^D_j(p)>=<\nu^D_i(p')|i\sigma_{\mu\lambda}q^\lambda[F_M(q^2)+F_E(q^2)\gamma_5]+(q^2\gamma_\mu-q_\mu\hat{q})[F_V(q^2)+F_A(q^2)\gamma_5]|\nu^D_j(p)>, \tag{8}$$

where $q=p'-p$, $F_M(q^2)$, $F_E(q^2)$, $F_A(q^2)$ and $F_V(q^2)$ are the magnetic, electric, anapole and reduced Dirac formfactors, respectively. In the static limit ($q^2=0$) $F_M(q^2)$ and $F_E(q^2)$ define (anomalous) dipole magnetic moment μ_{ij} and dipole electric moment d_{ij}, respectively. At $i=j$ and $q^2=0$, $F_A(q^2)$ represents the anapole neutrino moment.

For a Majorana neutrino all the formfactors, except the axial one F_A, are identically equal to zero. As regards non-diagonal elements, the situation depends on the fact whether CP-parity is conserved or not. For the CP non-variant case all the four formfactors are nonzero. When CP invariance takes place and the $|\nu^M_i>$- and $|\nu^M_j>$-states have identical (opposite) CP-parities, then $(F_E)_{ij}$ and $(F_A)_{ij}$ ($(F_M)_{ij}$ and $(F_V)_{ij}$) are different from zero.

By now we have information concerning the DMMs of ordinary left-handed neutrinos ν_{aL} while any experimental data associated with the DMMs of heavy right-handed neutrinos N_{aR} is absent. The most sensitive and established method for the experimental investigation of the neutrino DMMs is provided by direct laboratory measurements of electron (anti)neutrino-electron scattering at low energies in solar, accelerator and reactor experiments. The best limit was obtained in the work [4]

$$\mu_\nu\le 3.2\times 10^{-11}\mu_B.$$

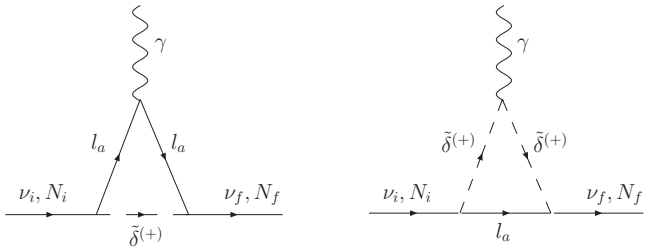

Figure 1. The Feynman diagrams caused by the virtual singly charged boson only.

Contributions to the neutrino DMMs coming from the diagrams with the virtual charged gauge bosons W_1 and W_2 have the following form [5]:

$$\mu_{ii'}^{\nu\nu} = -\frac{3g_L^2 m_e(m_{\nu_i} + m_{\nu_{i'}})\mu_B}{32\pi^2} \sum_a \left[\frac{\cos^2\xi}{m_{W_1}^2}\epsilon_a^{(1)} + \frac{\sin^2\xi}{m_{W_2}^2}\epsilon_a^{(2)} \right] \times \mathrm{Im}[U_{i'a}^\dagger U_{ai}], \tag{9}$$

$$\mu_{jj'}^{NN} = \mu_{ii'}^{\nu\nu}(g_L \to g_R, U_{ai} \to V_{aj}, m_{\nu_i} \to m_{N_j}, \xi \to \xi + \pi/2), \tag{10}$$

$$\mu_{ij}^{\nu N} = \frac{g_L g_R m_e \mu_B}{2\pi^2} \sin\xi\cos\xi \sum_a m_a \mathrm{Im}\left[e^{-i\phi}U_{ja}^\dagger V_{ai}\right] \left\{ \sum_{k=1}^{2} \frac{(-1)^k}{m_{W_k}^2} \left[1 + \epsilon_a^{(k)} \left(\ln\epsilon_a^{(k)} + \frac{9}{8} \right) \right] \right\}, \tag{11}$$

where

$$\nu_{iL} = U_{ia}^\dagger \nu_{aL}, \qquad N_{iR} = V_{ia}^\dagger N_{aR}, \qquad \epsilon_a^{(k)} = \frac{m_a^2}{m_{W_k}^2}, \qquad k = 1, 2,$$

and U_{ia} (V_{ia}) is the mixing matrix in the light (heavy) neutrino sector while ξ is the mixing angle in the charged gauge boson sector. Assuming that

$$g_L = g_R, \qquad m_{W_2} = 4 \text{ TeV}, \qquad \xi = 2 \times 10^{-4}, \tag{12}$$

and N_j, $N_{j'}$ are on the EWS, we obtain the small value for $\mu_{ii'}^{\nu\nu}$ as before, while

$$|\mu_{jj'}^{NN}| \approx 10^{-11}\mu_B \qquad \text{and} \qquad |\mu_{ij}^{\nu N}| \approx 2 \times 10^{-13}\mu_B. \tag{13}$$

Contributions to the neutrino DMM coming from the $\tilde{\delta}^{\pm}$-bosons were found in [6]. They are caused by the diagrams pictured on Fig. 1. The results are as follows ($i \neq f$)

$$(\mu^{\nu\nu})_{if} = \frac{m_e\mu_B}{2\pi^2} \sum_{l_a} \frac{\alpha_{\nu_a\tilde{\delta}l_a}\alpha_{\nu_a\tilde{\delta}l_a}}{(m_{\nu_i} - m_{\nu_f})} \int_0^1 xdx \left[\ln\left|\frac{M_{\nu_i\tilde{\delta}}}{M_{\nu_f\tilde{\delta}}}\right| + \ln\left|\frac{M_{\nu_i l_a}}{M_{\nu_f l_a}}\right| \right] \times \mathrm{Im}[(\mathcal{D}_{fl_a}^{\nu\nu})^\dagger \mathcal{D}_{l_a i}^{\nu\nu}], \tag{14}$$

$$(\mu^{NN})_{if} = (\mu^{\nu\nu})_{if}(\nu_i \longrightarrow N_i, \nu_f \longrightarrow N_f), \tag{15}$$

$$(\mu^{\nu N})_{if} = -\frac{m_e\mu_B}{2\pi^2} \sum_{l_a} \alpha_{N_a\tilde{\delta}l_a}\alpha_{\nu_a\tilde{\delta}l_a} m_{l_a} \int_0^1 dx \left[\frac{1}{m_{N_i}^2} \ln\left|\frac{M_{\nu_f\tilde{\delta}}}{M_{N_i\tilde{\delta}}}\right| - \right.$$
$$\left. - \frac{x}{m_{N_j}^2(1-x) + m_{\nu_i}^2 x} \ln\left|\frac{M_{\nu_i l_a}}{M_{N_j l_a}}\right| \right] \times \mathrm{Im}[\mathcal{U}_{jl_a}^\dagger \mathcal{U}_{l_a i}], \tag{16}$$

where

$$M_{N_i\tilde{\delta}} = (m_{\tilde{\delta}}^2 - m_{N_i}^2)x + m_{N_i}^2 x^2 + m_{l_a}^2(1-x), \qquad M_{N_i l_a} = (m_{l_a}^2 - m_{N_i}^2)x + m_{N_i}^2 x^2 + m_{\tilde{\delta}}^2(1-x).$$

$$M_{\nu_i l_a} = (m_{l_a}^2 - m_{\nu_i}^2)x + m_{\nu_i}^2 x^2 + m_{\tilde{\delta}}^2(1-x), \qquad M_{\nu_i\tilde{\delta}} = (m_{\tilde{\delta}}^2 - m_{\nu_i}^2)x + m_{\nu_i}^2 x^2 + m_{l_a}^2(1-x).$$

Besides the diagrams pictured on Fig.1 the contributions to the neutrino DMM come from diagrams shown on Fig.2.

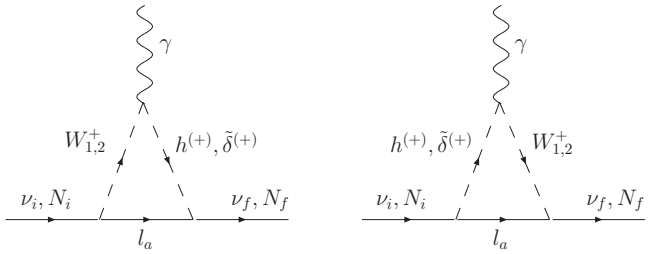

Figure 2. The Feynman diagrams caused by both the virtual singly charged boson and charged gauge boson.

These diagrams give the following contributions to the neutrino DMMs

$$(\mu'^{\nu\nu}_{\tilde{\delta}})_{ii'} = \frac{ig_L m_e \mu_B}{32\sqrt{2}\pi^2} \sum_{l_a} \alpha_{\nu_a \tilde{\delta} l_a} \alpha_{W\tilde{\delta}\gamma} \left\{ \frac{\sin 2\xi}{m^2_{W_1}} \int_0^1 dx \left[\frac{1}{M_{\nu_{i'}\tilde{\delta}} - M_{\nu_i W_1}} \ln \left| \frac{M_{\nu_{i'}\tilde{\delta}}}{M_{\nu_i W_1}} \right| \times \right.\right.$$
$$\times \left(x^2 m^2_{W_1} + 2(2x - 3x^2) M_{\nu_i W_1} + (x^3 - x^4)(m^2_{\nu_i} + m^2_{\nu_{i'}}) + x^2(m^2_{\nu_i} + \right.$$
$$\left. + m_{\nu_i} m_{\nu_{i'}}) \right) + 2(3x^2 - 2x) \left(\ln \left| \frac{l^\nu_h}{M_{\nu_{i'}\tilde{\delta}}} \right| + \frac{l^\nu_{W_1}}{l^\nu_{\tilde{\delta}} - l^\nu_{W_1}} \ln \left| \frac{l^\nu_{\tilde{\delta}}}{l^\nu_{W_1}} \right| \right) \Bigg] \times \mathrm{Im}[\mathcal{U}^\dagger_{i' l_a} \mathcal{U}_{l_a i}] -$$
$$\left. - (W_1 \longrightarrow W_2, \mathcal{U}^\dagger_{i' l_a} \longrightarrow \mathcal{U}^\dagger_{i' l_a} e^{i\phi}) \right\} + (m_{\nu_i} \leftrightarrow m_{\nu_{i'}}), \qquad (17)$$

$$(\mu'^{NN}_{\tilde{\delta}})_{jj'} = \frac{ig_L m_e \mu_B}{16\sqrt{2}\pi^2} \sum_{l_a} \alpha_{N_a \tilde{\delta} l_a} \alpha_{W\tilde{\delta}\gamma} \left\{ \frac{\cos^2 \xi}{m^2_{W_2}} \int_0^1 dx \left[\frac{1}{M_{N_{j'}\tilde{\delta}} - M_{N_j W_2}} \ln \left| \frac{M_{N_{j'}\tilde{\delta}}}{M_{N_j W_2}} \right| \times \right.\right.$$
$$\times \left(x^2 m^2_{W_2} + 2(2x - 3x^2) M_{N_j W_2} + (x^3 - x^4)(m^2_{N_j} + m^2_{N_{j'}}) + x^2(m^2_{N_j} + \right.$$
$$\left. + m_{N_j} m_{N_{j'}}) \right) + 2(3x^2 - 2x) \left(\ln \left| \frac{l^N_{\tilde{\delta}}}{M_{N_{j'}\tilde{\delta}}} \right| + \frac{l^N_{W_2}}{l^N_{\tilde{\delta}} - l^N_{W_2}} \ln \left| \frac{l^N_{\tilde{\delta}}}{l^N_{W_2}} \right| \right) \Bigg] \times \mathrm{Im}[\mathcal{U}^\dagger_{j' l_a} \mathcal{U}_{l_a j}] +$$
$$\left. + (W_2 \to W_1, \xi \to \xi + \pi/2, \mathcal{U}^\dagger_{j' l_a} \longrightarrow \mathcal{U}^\dagger_{j' l_a} e^{-i\phi}) \right\} + (m_{N_j} \leftrightarrow m_{N_{j'}}),$$
$$(\mu'^{\nu N}_{\tilde{\delta}})_{ij} = -\frac{ig_L m_e \mu_B}{64\sqrt{2}\pi^2} \sum_{l_a} \alpha_{W\tilde{\delta}\gamma} \alpha_{N_a \tilde{\delta} l_a} m_{l_a} \left\{ \frac{\sin 2\xi}{m^2_{W_1}} \int_0^1 \frac{dx}{M_{N_j\tilde{\delta}} - M_{\nu_i W_1}} \ln \left| \frac{M_{N_j\tilde{\delta}}}{M_{\nu_i W_1}} \right| \times \left[x^3(m_{N_j} + m_{\nu_i}) - \right.\right.$$
$$\left. - x^2(3m_{\nu_i} + m_{N_j}) + 2x m_{\nu_i} \right] \times \mathrm{Im}[e^{-i\phi} \mathcal{U}^\dagger_{j l_a} \mathcal{U}_{l_a i}] + (W_1 \longrightarrow W_2, \phi \longrightarrow 0) \Bigg\} + (m_{N_j} \leftrightarrow m_{\nu_i}), \qquad (18)$$

where

$$l^\nu_{W_k} = (m^2_{W_k} - m^2_{\nu_i})x + m^2_{l_a}(1 - x), \qquad l^N_{W_k} = l^\nu_{W_k}(\nu_i \to N_j),$$
$$l^\nu_{\tilde{\delta}} = (m^2_{\tilde{\delta}} - m^2_{\nu_i})x + m^2_{l_a}(1 - x), \qquad l^N_{\tilde{\delta}} = l^\nu_{\tilde{\delta}}(\nu_i \to N_j), \qquad l^\nu_{W_k} + m^2_{\nu_i} x^2 = M_{\nu_i W_k},$$
$$M_{\nu_i \tilde{\delta}} = l^\nu_{\tilde{\delta}} + m^2_{\nu_i} x^2, \qquad M_{N_j W_k} = M_{\nu_i W_k}(\nu_i \to N_j), \qquad l^N_{\tilde{\delta}} + m^2_{N_j} x^2 = M_{N_j \tilde{\delta}}.$$

Let us estimate the expressions for the DMMs obtained in this work using the values of the LRM parameters (12) and assuming that $m_{\tilde{\delta}} = 100$ GeV. As will be shown later, in the heavy neutrino sector only two scenarios are possible: (i) the heavy neutrino masses are (quasi) degenerated and the mixing angles between heavy and light neutrinos are equal (quasi mass degeneracy — QMD); (ii) the heavy neutrino masses are arbitrary and the mixing inside the same generation is absent (no mass degeneracy — NMD). Then, we get

$$(\mu^{\nu\nu})_{if} \approx -10^{-12} \mu_B, \qquad (\mu^{NN})_{if} \approx -5 \times 10^{-13} \mu_B, \qquad (\mu^{\nu N})_{if} \approx 10^{-10} \mu_B$$

for the QMD case and

$$(\mu^{\nu\nu})_{if} \approx -5 \times 10^{-11} \mu_B, \qquad (\mu^{NN})_{if} \approx 10^{-8} \mu_B, \qquad (\mu^{\nu N})_{if} \approx 10^{-8} \mu_B$$

for the NMD case.

3 Phenomenology of heavy neutrinos

Let us consider the motion of the high-energy beam of the left-handed electron neutrinos in matter and a twisting magnetic field. We shall be constrained by the two flavor approximation. The object of our investigation represents the system with the wave function $\Psi^T = (\nu_{eL}, \nu_{\mu L}, N_{eR}, N_{\mu R})$ and with the mixing matrix of the form

$$\mathcal{U} = \begin{pmatrix} \cos\theta_{12}^{\nu} & \sin\theta_{12}^{\nu} & 0 & 0 \\ -\sin\theta_{12}^{\nu} & \cos\theta_{12}^{\nu} & 0 & 0 \\ 0 & 0 & \cos\theta_{12}^{N} & \sin\theta_{12}^{N} \\ 0 & 0 & -\sin\theta_{12}^{N} & \cos\theta_{12}^{N} \end{pmatrix} \begin{pmatrix} \cos\theta_{11} & 0 & \sin\theta_{11} & 0 \\ 0 & \cos\theta_{22} & 0 & \sin\theta_{22} \\ -\sin\theta_{11} & 0 & \cos\theta_{11} & 0 \\ 0 & -\sin\theta_{22} & 0 & \cos\theta_{22} \end{pmatrix}. \tag{19}$$

The corresponding Hamiltonian is determined by the expression

$$\mathcal{H} = \begin{pmatrix} \mathcal{H}_{\nu\nu} & \mathcal{H}_{\nu N} \\ \mathcal{H}_{\nu N}^{\dagger} & \mathcal{H}_{NN} \end{pmatrix}, \tag{20}$$

where

$$\mathcal{H}_{\nu\nu} = \begin{pmatrix} c_{\theta_{11}}^2\Delta_c^{\nu} + s_{\theta_{11}}^2\Delta_c^{N} + c_{2\theta_{11}}\Sigma + V_{eL} - \dot{\Phi}/2 & c_{\theta_{11}}c_{\theta_{22}}\Delta_s^{\nu} + s_{\theta_{11}}s_{\theta_{22}}\Delta_s^{N} + \mu_{\nu_e\nu_\mu}B_{\perp} \\ c_{\theta_{11}}c_{\theta_{22}}\Delta_s^{\nu} + s_{\theta_{11}}s_{\theta_{22}}\Delta_s^{N} + \mu_{\nu_e\nu_\mu}B_{\perp} & -c_{\theta_{22}}^2\Delta_c^{\nu} - s_{\theta_{22}}^2\Delta_c^{N} + c_{2\theta_{22}}\Sigma + V_{\mu L} - \dot{\Phi}/2 \end{pmatrix},$$

$$\mathcal{H}_{\nu N} = \begin{pmatrix} \frac{s_{2\theta_{11}}}{2}(\Delta_c^{N} - \Delta_c^{\nu} - 2\Sigma) + \mu_{\nu_e N_e}B_{\perp} & s_{\theta_{11}}c_{\theta_{22}}\Delta_s^{N} - c_{\theta_{11}}s_{\theta_{22}}\Delta_s^{\nu} + \mu_{\nu_e N_\mu}B_{\perp} \\ c_{\theta_{11}}s_{\theta_{22}}\Delta_s^{N} - s_{\theta_{11}}c_{\theta_{22}}\Delta_s^{\nu} + \mu_{\nu_e N_\mu}B_{\perp} & \frac{s_{2\theta_{22}}}{2}(\Delta_c^{\nu} - \Delta_c^{N} - 2\Sigma) + \mu_{\nu_\mu N_\mu}B_{\perp} \end{pmatrix},$$

$$\mathcal{H}_{NN} = \mathcal{H}_{\nu\nu}\big(\theta_{11} \to \theta_{11} + \frac{\pi}{2}, \theta_{22} \to \theta_{22} + \frac{\pi}{2}, V_{eL} \to V_{eR}, V_{\mu L} \to V_{\mu R}, \dot{\Phi} \to -\dot{\Phi}\big),$$

$$\Delta_{c(s)}^{\nu} = \frac{m_{\nu_2}^2 - m_{\nu_1}^2}{4E}\cos 2\theta_{12}^{\nu}(\sin 2\theta_{12}^{\nu}), \qquad \Delta_{c(s)}^{N} = \frac{m_{N_2}^2 - m_{N_1}^2}{4E}\cos 2\theta_{12}^{N}(\sin 2\theta_{12}^{N}),$$

$$\Sigma = \frac{m_{\nu_1}^2 + m_{\nu_2}^2 - m_{N_1}^2 - m_{N_2}^2}{8E}, \qquad c_{2\theta_{kk}} = \cos 2\theta_{kk}, \qquad k = 1, 2,$$

V_{eL} (V_{eR}) and $V_{\mu L}$ ($V_{\mu R}$) are the matter potentials (MPs) describing the matter interaction with the left(right)-handed electron neutrino and muon neutrino:

$$V_{eL} = \sqrt{2}G_F(N_e - N_n/2) + V_{eL}^H, \qquad V_{\mu L} = -\sqrt{2}G_F N_n/2 + V_{\mu L}^H,$$
$$V_{eR} = \frac{g^2 N_e}{4m_{W_2}^2} - \frac{g^2 c_{\theta_W}^2 N_n}{8(c_{\theta_W}^2 - s_{\theta_W}^2)m_{Z_2}^2}, \quad V_{\mu R} = -\frac{g^2 c_{\theta_W}^2 N_n}{8(c_{\theta_W}^2 - s_{\theta_W}^2)m_{Z_2}^2}, \quad V_{aL}^H = \left(\frac{\alpha_{ea}^2}{2m_h^2} - \frac{f_{ea}^2}{m_{\tilde{\delta}}^2}\right)N_e, \tag{21}$$

where N_e (N_n) is the density of electrons (neutrons), $c_{\theta_W} = \cos\theta_W$, $s_{\theta_W} = \sin\theta_W$, θ_W is the Weinberg angle and we have neglected the mixing in the gauge boson sector.

Equalling the corresponding elements of the Hamiltonian (20), we can find all the totality of the resonance conversions in the case under consideration. Under fulfillment of the condition

$$V_{eL} - V_{\mu L} = -(c_{22}^2 + c_{11}^2)\Delta_c^{\nu} - (s_{22}^2 + s_{11}^2)\Delta_c^{N} + (c_{2\theta_{22}} - c_{2\theta_{11}})\Sigma \tag{22}$$

the $\nu_{eL} \to \nu_{\mu L}$-resonance (Mikheyev-Smirnov-Wolfenstein — MSW) occurs. Since the description of the MSW-resonance within the SM is sufficiently successful, then corrections to the SM predictions must be small in any SM extensions. Let us find out constraints on the LRM parameters that follow from this demand. The right-handed side of Eq. (22) will be close to the SM predictions in two cases: (i) the heavy neutrino masses m_{N_1} and m_{N_2} are arbitrary while the mixing inside generations is absent (NMD)

$$\theta_{11} = \theta_{22} = 0; \tag{23}$$

(ii) the angles θ_{11} and θ_{22} are equal to each other but not equal to zero whereas the heavy neutrino masses are (quasi)degenerated (QMD)

$$\theta_{11} = \theta_{22} \qquad \text{and} \qquad (m_{N_2}^2 - m_{N_1}^2)\cos 2\theta_{12}s_{22}^2 \approx (m_{\nu_2}^2 - m_{\nu_1}^2). \tag{24}$$

If the conditions

$$V_{eL} - V_{eR} - \dot{\Phi} = (\delta_c^{21} - \delta_c^{43})(s_e^2 - c_e^2) - 2c_{2\theta_e}\Delta, \tag{25}$$

and

$$V_{eL} - V_{eR} - \dot{\Phi} = -\delta_c^{21}(c_e^2 + s_\mu^2) - \delta_c^{43}(s_e^2 + c_\mu^2) - \Delta(c_{2\theta_e} + c_{2\theta_\mu}) \tag{26}$$

are fulfilled, we would have the $\nu_{eL} \to N_{eR}$- and $\nu_{eL} \to N_{\mu R}$ resonance transitions, respectively. It is clear that both the NMD- and QMD-schemes do not allow the existence of this resonances. So we may conclude, in spite of rather big values of $\mu_{ij}^{\nu N}$, in oscillation experiments with left-handed light neutrinos beam we have not the ghost of a chance to observe the heavy neutrinos production even at energies $E_\nu > m_N$.

Now we proceed to collider experiments. First we consider the process of the heavy neutrino production under collision of light neutrino beam with the proton target

$$\nu_{\mu L} + p \to \gamma^* \to N_{\mu R} + X, \tag{27}$$

where X is a nondetecting hadron state. The corresponding subprocesses are

$$\nu_{\mu L} + q_i \to \gamma^* \to N_{\mu R} + q_i, \tag{28}$$

$$\nu_{\mu L} + \overline{q}_i \to \gamma^* \to N_{\mu R} + \overline{q}_i. \tag{29}$$

Let us set the light neutrino mass equal to zero and do not take interest in the polarization of the initial and final particles. Calculations lead to the following value of the total cross section

$$\sigma(\nu_\mu p \to N_\mu X) = \frac{2\alpha^2|\mu^{\nu N}|^2\pi}{\mu_B^2 m_e^2 s^2} \sum_{q_i} n_{q_i}^2 \int_0^1 \frac{dx}{x^2} \left[f_{q_i}(x) + f_{\overline{q}_i}(x)\right] \left[2m_N^2 xs - 2x^2 s^2 - \right.$$
$$\left. -2m_{q_i}^4 - m_N^4\right] \ln\left|\frac{\beta_+(xs)}{\beta_-(xs)}\right| + \left[\beta_+(xs) - \beta_-(xs)\right]\left(2m_{q_i}^2 - 2xs + m_N^2 - \frac{2m_N^4 m_{q_i}^2}{\beta_+(xs)\beta_-(xs)}\right], \tag{30}$$

where s is the total energy squared of the colliding ν_μ-neutrino and proton in the center-of-mass frame, $f_{q_i}(x)$ and $f_{\overline{q}_i}(x)$ are the distribution functions of quarks and antiquarks inside the proton. When $\mu^{\nu N} = 10^{-8}\mu_B$ and $s = 10$ TeV, we have $\sigma(\nu_\mu p \to N_\mu p X) \approx 10$ fb. It is clear that at the existing experiment technique we could detect this process.

Further we consider possibilities of the observation of the transit DMM of the heavy neutrino at LHC. We start with the single heavy neutrino production in the process

$$p + p \to \gamma^* \to N_e + \overline{\nu}_e + X. \tag{31}$$

The differential cross section for the corresponding subprocess is given by the expression

$$\frac{d\hat{\sigma}}{d\hat{t}}(q_i\overline{q}_i \to N_e\overline{\nu}_e) = \frac{2n_{q_i}^2\alpha^2|\mu^{\nu N}|^2\pi}{m_e^2\mu_B^2\hat{s}^4}\left\{2\hat{s}\hat{u}\hat{t} + \hat{s}^2(m_N^2 + 2m_{q_i}^2) - \hat{s}(2m_{q_i}^4 + m_N^4) - 2m_N^4 m_{q_i}^2\right\}. \tag{32}$$

To integrate the expression (32) gives

$$\hat{\sigma}(q_i\overline{q}_i \to N_e\overline{\nu}_e) = \frac{2n_{q_i}^2\alpha^2|\mu^{\nu N}|^2\pi}{m_e^2\mu_B^2\hat{s}^4}\left\{\frac{\hat{s}^4}{3} + 2m_{q_i}^2\hat{s}^3 - \hat{s}^2\left[m_N^4 + 2m_N^2 m_{q_i}^2 + 2m_{q_i}^4\right] + \right.$$
$$\left. +2\hat{s}\left[\frac{m_N^6}{3} - m_N^4 m_{q_i}^2 + m_N^2 m_{q_i}^4\right] + 2m_N^6 m_{q_i}^2\right\}. \tag{33}$$

With the help of the obtained expression one can find $\sigma(pp \to \overline{\nu}_e N_e X)$. At the LHC energies and $\mu^{\nu N}$ being equal to $10^{-8}\mu_B$ the cross section of the reaction (31) is in the region of very small values 10^{-2} fb.

Let us approach to the problem of detecting the transit DMM $\mu^{\nu N}$ on the other hand. With zero value of $\mu^{\nu N}$, the dominant decay channel of the heavy neutrino is

$$N_a \to l_a + W_R^* \to l_a + 2j. \tag{34}$$

The corresponding decay width is defined by the expression

$$\Gamma(N \to lW_R^* \to ljj) \simeq N_c \frac{g_R^4 m_N^5}{1024\pi^3 m_{W_R}^4} \tag{35}$$

where the fermion masses have been neglected and the both lepton channels $\Gamma(N \to l^+ W_R^{-*}) = \Gamma(N \to l^- W_R^{+*})$ have been summed. However, if the $\mu_{ij}^{\nu N}$ moment has nonzero value, the heavy neutrino may also decay into the channel

$$N_l \to \gamma + \nu_l. \tag{36}$$

The decay width will look like

$$\Gamma(N_l \to \gamma\nu_l) = \frac{2\alpha|\mu^{\nu N}|^2 m_{N_l}^3}{\mu_B^2 m_e^2}. \tag{37}$$

We see that when $m_{N_l} = 100$ GeV and $\mu^{\nu N} = 10^{-8}\mu_B$ the decay width $\Gamma(N_{l_a} \to \gamma\nu_{l_a})$ could exceed $\Gamma(N_{l_a} \to \gamma l_a 2j)$ over several orders of magnitude. Note, that the DMM $\mu^{\nu N}$ rapidly decreases with the growth of m_N and in the region of $m_N \approx 300$ GeV the both decay widths have the same order of magnitude $\sim 10^{-6}$ GeV. Further one may choose the process of the heavy neutrino production having the most cross section and detect the heavy neutrino through the decay channel (36).

At LHC there are two possibilities for observing the heavy neutrino production. The former is the single heavy neutrino production that may take place due to the reaction

$$p + p \to W_R^* \to e^+ + N_e + X. \tag{38}$$

At $m_{W_R} = 4$ TeV, the cross section of this reaction is as high as 3×10^{-3} pb. This estimate of $\sigma(pp \to eN_eX)$ is valid for $m_N = 100$ GeV and are not practically changed to the extent $m_N \simeq 0.6 m_{W_R}$. Pair production of heavy neutrinos take place in the reaction

$$p + p \to Z_R^* \to N_e + \overline{N}_e + X. \tag{39}$$

Supposing the fulfillment of $m_{Z_R} = 1.7 m_{W_R} = 6.8$ TeV we have

$$\sigma(pp \to Z_R^* \to N_e N_e X) \simeq 3 \times 10^{-5} \text{ pb}. \tag{40}$$

The value (40) is also given for $m_N = 100$ GeV and it is weakly changed up to $m_N \simeq 0.4 m_{Z_R}$. So, we see, that for detecting heavy neutrinos the reaction (38) is the most perspective.

For m_{N_a} in the range of several hundreds GeV, the total N_a width is at most a few percents of m_a. Thus, we can take the narrow width approximation:

$$\sigma(pp \to W_R^* \to eN_e \to e\nu_e\gamma) \simeq \sigma(pp \to W_R^* \to eN_e) Br(N_e \to \nu_e\gamma). \tag{41}$$

Then, assuming that $m_{N_e} = 100$ GeV, $m_{W_R} = 4$ TeV and $\mu^{\nu N} = 10^{-8}\mu_B$, we obtain

$$\sigma(pp \to W_R^* \to eN_e \to e\nu_e\gamma) \simeq 3 \text{ fb}. \tag{42}$$

So, under the integrated luminosity $\int Ldt = 10$ fb^{-1} we shall observe 30 events. However, under increasing the heavy neutrino mass $Br(N_e \to \nu_e\gamma)$ is sharply decreased. For example, when $m_{N_e} = 300$ GeV there will be 15 events only.

Let us proceed to detection of μ^{NN}. We address to the pair production of the heavy neutrinos taking into account the DMM μ^{NN}. Then, we shall have

$$p + p \to Z_R^*, \gamma^* \to N_a + \overline{N}_b + X. \tag{43}$$

Note, that the weak and electromagnetic diagrams do not interfere. The corresponding subprocesses are as follows

$$q_i + \overline{q}_i \to Z_R^* \to N_a + N_b, \tag{44}$$

$$q_i + \overline{q}_i \to \gamma^* \to N_a + N_b \tag{45}$$

The cross section of (45) looks like

$$\sigma_{em} = \frac{2\alpha^2 |\mu^{N_a N_b}|^2 \pi}{3\mu_B^2 m_e^2} \sqrt{1 - \frac{4m_{N_a}^2}{s}}. \tag{46}$$

When $\mu^{NN} \approx 10^{-8}\mu_B$ and $m_{Z_R} = 6.8$ TeV, then the ratio

$$R = \sigma(pp \to \gamma^* \to N_a\overline{N}_a)/\sigma(pp \to Z_R^* \to N_a\overline{N}_a)$$

is close to one.

4 Conclusion

Within the left-right-symmetric model contributions to the neutrino dipole magnetic moments coming from the sectors of the gauge bosons and Higgs bosons have been considered. It has been shown that the contributions caused by the singly charged $\tilde{\delta}^{(\pm)}$-Higgs bosons could exceed that caused by the charged gauge bosons.

Investigation of the resonance conversion $\nu_{eL} \to \nu_{\mu L}$ (Mikheyev-Smirnov-Wolfenstein resonance) has revealed that in the heavy neutrino sector only two scenarios could be realized: (i) the heavy neutrino masses are quasi-degenerated and the mixing angles between heavy and light neutrinos are equal; (ii) the heavy neutrino masses are arbitrary and the mixing inside the same generation is absent.

It was proven that in oscillation experiments with left-handed light neutrinos beam we cannot observe the heavy neutrinos production even at energies $E_\nu > m_N$.

In collider experiments we can detect both the μ^{NN} and $\mu^{\nu N}$ moments. The most promising reactions are as follows

$$\nu_{\mu L} + p \to N_{\mu R} + X \qquad (\sigma \leq 10 \text{ fb}),$$
$$p + p \to \gamma^* \to N_{eR} + \overline{\nu}_{eL} + X \qquad (\sigma \leq 10^{-2} \text{ fb}).$$

The nonzero value of $\mu^{\nu N}$ could be also observed through the decay

$$N_{eR} \to \gamma^* \to \nu_{eL}.$$

A good example is the process

$$p + p \to W_R^* \to e + N_e \to e + \nu_e + \gamma + X.$$

Using the narrow width approximation we get

$$\sigma(pp \to W_R^* \to eN_e \to e\nu_e\gamma) \simeq \sigma(pp \to W_R^* \to eN_e)Br(N_e \to \nu_e\gamma) \leq 3 \text{ fb}.$$

References

[1] O.M.Boyarkin *Advanced Particles Physics, Volume II* (Taylor and Francis Group, New York, 2011).
[2] J.C.Pati and A.Salam, Phys. Rev. **D10**, 275 (1974).
[3] G.Boyarkina, O.Boyarkin, Eur. Phys. J. **C13**, 99, 2000.
[4] A.G.Beda *et al.*, Phys. Part. Nucl. Lett. **7**, 406 (2010).
[5] J.Kim, Phys. Rev. **D14**, 3000 (1976).
[6] O.M.Boyarkin, G.G.Boyarkina, Phys. Atom. Nucl. **76**, 504 (2013).

Proceedings of the International School-seminar
"New Physics and Quantum Chromodynamics at External Conditions", pp. 57 – 64,
May 22-24, 2013, Dnipropetrovsk, Ukraine

CHIRAL SYMMETRY BREAKING AND CENTER VORTICES

M. Faber[a], R. Höllwieser[b]

Institute of Atomic and Subatomic Physics, Vienna University of Technology, Operngasse 9, 1040 Vienna, Austria

We investigate the chiral properties of near-zero modes for thick classical center vortices in $SU(2)$ lattice gauge theory as examples of the phenomena which may arise in a vorex vacuum. In particular we analyze the creation of near-zero modes from would-be zero modes of various topological charge contributions from center vortices. We show that colorful spherical vortex and instanton ensembles have very similar Dirac eigenmodes and also vortex intersections are able to give rise to a finite density of near-zero modes, leading to chiral symmetry breaking via the Banks-Casher formula. We discuss the influence of the magnetic vortex fluxes on quarks and how center vortices may break chiral symmetry.

1 Introduction

The breaking of chiral symmetry is an effect which is strongly related to the structure of the non-perturbative vacuum of QCD. The only method at present available to tackle this non-perturbative problem is lattice QCD (LQCD). A well established theory of χSB relies on instantons [1–3], which are localized in space-time and carry a topological charge of modulus 1. According to the Atiyah-Singer index theorem [4], a zero mode of the Dirac operator arises, which is concentrated at the instanton core. In the instanton liquid model [5, 6] overlapping would-be zero modes split into low-lying nonzero modes which create the chiral condensate. Center vortices [7], closed magnetic flux tubes, are promising candidates for explaining confinement. The vortex model of confinement is theoretically appealing and was confirmed by a multitude of numerical calculations, both, in lattice Yang-Mills theory and within a corresponding infrared effective model, see *e.g.* [8, 9]. Lattice simulations indicate that vortices are responsible for topological charge and χSB as well [10–12], and thus unify all nonperturbative phenomena in a common framework. A similar picture to the instanton liquid model exists insofar as lumps of topological charge arise at the intersection and writhing points of vortices. The colorful, spherical SU(2) vortex was introduced in previous article of our group [13] and may act as a prototype for this picture, as it contributes to the topological charge by its color structure, attracting a zero mode like an instanton. We show how the interplay of various topological structures from center vortices (and instantons) leads to near-zero modes, which by the Banks-Casher relation [14] are responsible for a finite chiral condensate. We compute a varying number of the lowest-lying overlap Dirac eigenfunctions and visualize their chiral density.

2 Free Dirac eigenmodes

Fig. 1 shows the chiral density of free overlap eigenmodes obtained numerically using the MILC code. The modes are found with the Ritz functional algorithm [15, 16] with random start and for degenerate eigenvalues the eigenmodes span a randomly oriented basis in the degenerate subspace. Therefore the numerical modes presented in Fig. 1 are linear combinations of plane waves with momenta $\pm p_\mu$ and show plane wave oscillations of $2p_\mu$ in the chiral density. The first eight degenerate modes consist of plane waves with $p_4 = \pm\pi/24$, hence there is one sine (cosine) oscillation in time direction, the next eight have $p_4 = \pm 3\pi/24$, *i.e.*, three oscillations in the time direction. The oscillations of χ_R and χ_L are separated by half an oscillation length, *i.e.*, the maxima of ρ_+ correspond to minima of ρ_- and vice versa. Accordingly, the scalar density $\rho(x_\mu) = \frac{1}{2}(\chi_R^\dagger(x_\mu)\chi_R(x_\mu) + \chi_L^\dagger(x_\mu)\chi_L(x_\mu)) = 1/N_V$ is constant ($N_V \ldots$ lattice volume).

3 The Colorful Spherical Vortex

The spherical vortex was introduced in [13] and analyzed in more detail in [17] and [18]. It is constructed with t-links in a single time slice at fixed $t = t_i$, given by $U_t(x^\nu) = \exp\left(\mathrm{i}\alpha(|\vec{r} - \vec{r}_0|)\vec{r}/r \cdot \vec{\sigma}\right)$, where $\vec{r}$ is the spatial part of x_ν. The profile function $\alpha(r)$ changes from π to 0 in radial direction for the negative spherical vortex, or from π to 2π for the positive (anti-)vortex. This gives a hedgehog- like configuration, since the color vector points in (or against) the radial direction at the vortex radius R. The hedgehog-like structure is crucial for our

e-mail: [a]faber@kph.tuwien.ac.at, [b]hroman@kph.tuwien.ac.at

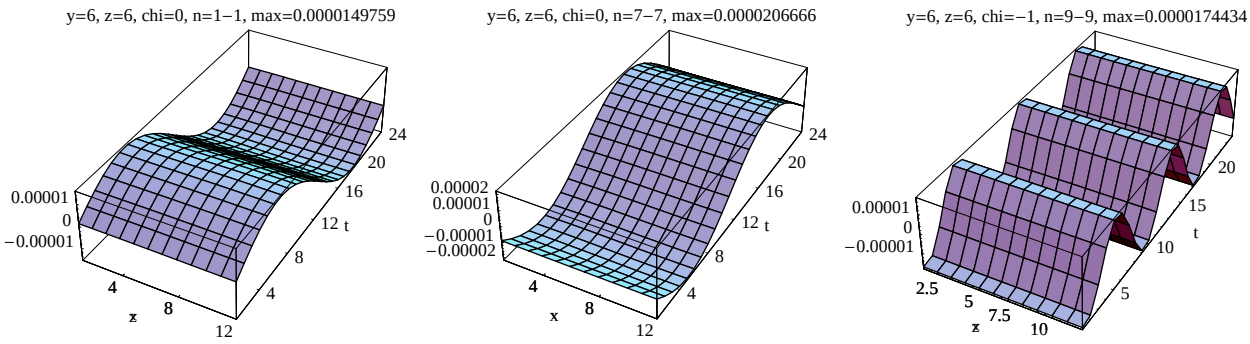

Figure 1. Chiral density of the low-lying eigenmodes of the free overlap Dirac operator: $\rho_5\#1$ (left), $\rho_5\#7$ (center) $\rho_5\#9$ (right). The modes clearly show the plane wave behavior with oscillations of $2p_\mu$ (see text).

analysis. The t-links of the spherical vortex define a map $S^3 \to SU(2)$, characterized by a winding number

$$N = -\frac{1}{24\pi^2}\int d^3x\, \epsilon_{ijk}\, \mathrm{Tr}[(U^\dagger\partial_i U)(U^\dagger\partial_j U)(U^\dagger\partial_k U)], \tag{1}$$

resulting in $N = -1$ for positive (anti-) and $N = +1$ for negative spherical vortices. Obviously such windings influence the Atiyah-Singer index theorem giving a topological charge $Q = -1$ for positive and $Q = +1$ for negative spherical vortices (anti-vortices). Hence, spherical vortices attract Dirac zero modes similar to instantons. In [18] we showed that the spherical vortex is in fact a vacuum-to-vacuum transition in the time direction which can even be regularized to give the correct topological charge also from gluonic definitions. In Fig. 2a we see that a single instanton has nearly exactly the same eigenvalues as a single spherical vortex. We interpreted the nonzero modes as eigenmodes of the free Dirac operator, which are shifted slightly because of their interaction with the nontrivial gauge field content. In Fig. 5 we show that even the chiral densities of the lowest eigenmodes distribute similarly, except for the fact that the response of the fermions to the spherical vortex is squeezed in the time direction, since the vortex is localized in a single time slice ($t = 5$). Another interesting issue is that the nonzero eigenmodes show plane wave oscillations, like the free eigenmodes in Fig. 1. We further plot the spectra of instanton–anti-instanton, spherical vortex-anti-vortex and instanton-anti-vortex pairs in Fig. 2a. We again see nearly exactly the same eigenvalues for instanton or spherical vortex pairs, but now we get instead of two would-be zero modes a near-zero mode for each pair. The chiral density plots in Fig. 6 for the instanton–anti-instanton pair and Fig. 7 for the spherical vortex-anti-vortex pair show, besides the similar densities, that the near-zero mode is a result of two chiral parts corresponding to the two constituents of the pairs. The nonzero modes can again be identified with the free overlap modes with the same side remark for mode #8. Finally in Fig. 2b we plot the eigenvalues of two (anti-)instantons and two spherical (anti-)vortices

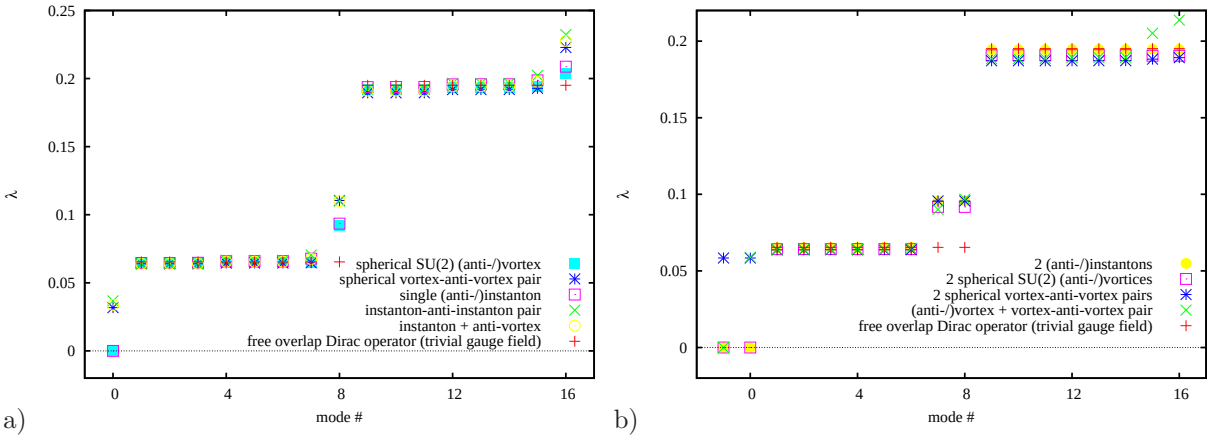

Figure 2. The lowest overlap eigenvalues for instanton and spherical vortex configurations compared to the eigenvalues of the free (overlap) Dirac operator.

giving topological charge $Q = 2$ ($Q = -2$) and therefore two zero modes, two vortex-anti-vortex pairs with two near-zero modes and a configuration with two vortices and an anti-vortex (*i.e.*, a single vortex plus one vortex-anti-vortex pair) giving one zero mode ($Q = 1$) and one near-zero mode. The results clearly show that

we may draw the same conclusions for spherical vortices as for instantons concerning the creation of near-zero modes.

4 Plane vortices

We define plane vortices parallel to two of the coordinate axes by links varying in a $U(1)$ subgroup of $SU(2)$. This $U(1)$ subgroup is generated by one of the Pauli matrices σ_i, *i.e.*, $U_\mu = \exp(\mathrm{i}\phi\sigma_i)$. Upon traversing a vortex sheet, the angle ϕ increases or decreases by π within a finite thickness of the vortex. Since we use periodic (untwisted) boundary conditions for the links, vortices occur in pairs of parallel sheets, each of which is closed by virtue of the lattice periodicity. We call vortex pairs with the same vortex orientation parallel vortices and vortex pairs of opposite flux direction anti-parallel. If thick, planar vortices intersect orthogonally, each intersection carries a topological charge $|Q| = 1/2$, whose sign depends on the relative orientation of the vortex fluxes [19], see Fig. 3. Fig. 3b indicates the position of the vortices after center projection, leading to (thin) P-vortices at half the thickness [8].

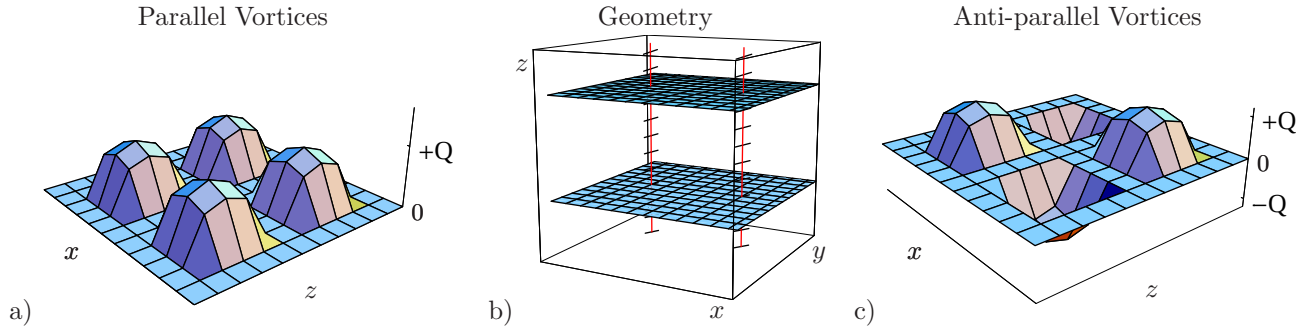

Figure 3. A single time-slice of a 12^4-lattice with intersecting vortices (center). The horizontal planes are the xy-vortices, which exist only at this time. The vertical lines are the zt-vortices, which continue over the whole time axis. The vortices intersect in four points, giving topological charge $Q = 2$ for parallel vortices (lhs) or $Q = 0$ for anti-parallel vortices (rhs).

For the configuration in Fig. 3a we get two real zero modes, according to the total topological charge $Q = 2$ of the four intersections. These modes we analyzed in [20], they peak at least at two of the four topological charge contributions of $Q = 1/2$. If we intersect anti-parallel vortex pairs orthogonally we get two intersection points with topological charge $Q = +1/2$ and two intersection points with topological charge $Q = -1/2$ (Fig. 3b), hence total $Q = 0$. For such a configuration we get four real near-zero modes, with local chirality peaks at the intersection points, according to their topological charge contribution, see Fig. 4b and compare to Fig. 3 c. Now, the mechanism of Sec. 3 or the analog instanton liquid model does not directly apply to the case of planar vortices, since there are no localized lumps of topological charge $Q = \pm 1$. Nevertheless the vortices attract chiral (near-)zero modes via their intersections with topological charge $Q = \pm 1/2$, which can be related to merons [21] and calorons [22]. We expect that vortex intersections, writhing points and even color structure contributions of vortices to topological charge are able to create a finite density of near-zero modes and break chiral symmetry via the Banks-Casher relation.

5 Conclusions

Fermions do not seem to make much of a difference between instantons and spherical vortices and the instanton liquid model can be extended to colorful spherical center vortices. Further also vortex intersections attract (would-be) zero modes which contribute via interactions to a finite density of near-zero modes with local chiral properties, *i.e.*, local chirality peaks at corresponding topological charge contributions. In Monte Carlo configurations we do not, of course, find perfectly flat or spherical vortices, as one does not find perfect instantons. The general picture of topological charge from vortex intersections, writhing points and even color structure contributions or instantons can provide a general picture of χSB: any source of topological charge can attract (would-be) zero modes and produce a finite density of near-zero modes leading to chiral symmetry breaking via the Banks-Casher relation. Here one also has to ask what could be the dynamical explanation of χSB. We can try the conjecture that only a combination of color electric and magnetic fields leads to χSB, electric fields accelerating color charges and magnetic fields trying permanently to reverse the momentum directions on spiral shaped paths. Such reversals of momentum keeping the spin of the particles should especially happen for very slowly moving color charges. Alternatively we could argue that magnetic color charges are able to flip the spin of slow quarks, *i.e.* when they interact long enough with the vortex structures. Finally, it seems that vortices not only confine quarks into bound states but also change their helicity in analogy to the instanton liquid model. In accordance with Casher's argument, a force strong enough to confine quarks is also generally expected to break

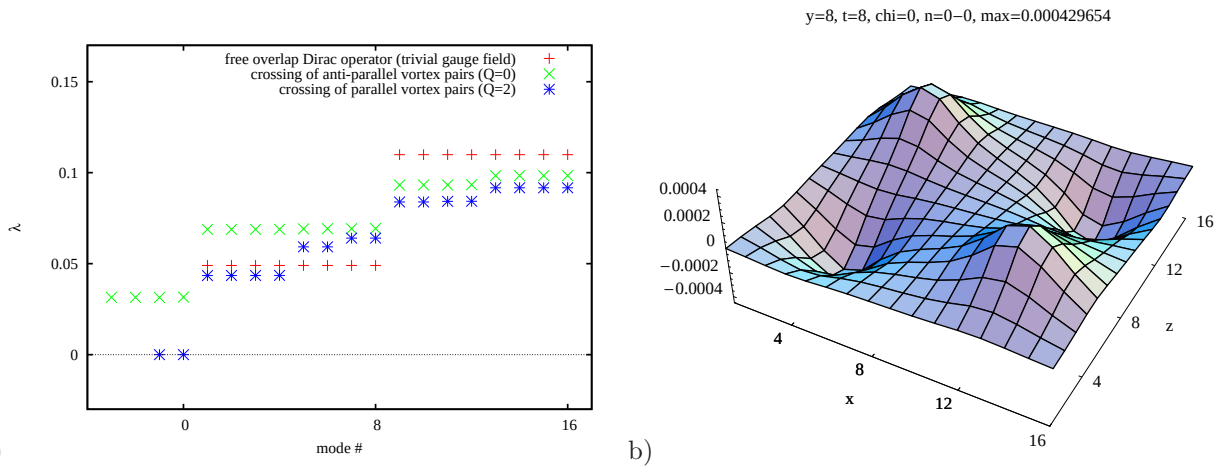

Figure 4. a) The lowest overlap eigenvalues for plane vortex configurations compared to the eigenvalues of the free (overlap) Dirac operator (red crosses) and spherical vortex configurations. b) Chiral density $\rho_5\#0$ in the intersection plane of all four near-zero modes of crossing flat vortex pairs with opposite flux direction ($Q = 0$).

chiral symmetry [23], we therefore conclude that the center vortex model of quark confinement may indeed be capable of describing chiral symmetry breaking. We should also mention that other mechanisms of chiral symmetry breaking in addition to the instanton liquid paradigm may be operative in the Yang-Mills vacuum. For instance, it also seems possible that, even in the absence of would-be zero modes, the random interactions of quarks with the vortex background may be strong enough to smear the free dispersion relation such that a finite Dirac operator spectral density at zero virtuality is generated. In fact, a confining interaction by itself generates chiral symmetry breaking, independent of any particular consideration of would-zero modes connected to topological charge. However, this effect on its own is not sufficiently strong for a quantitative explanation of the chiral condensate; other effects, among them possibly the ones considered in this article, must play a role. We cannot give a conclusive answer to the question of a dynamical explanation for the mechanism of χSB and only speculate on the importance of our results for Monte Carlo configurations, since there vortices are neither perfectly flat nor spherical, as there are no perfect instantons either. But the importance of the long-range nature of low-dimensional topological structures for the understanding of the mechanism of χSB in QCD was underlined by various results of different groups [24–30], and agrees well with a vortex picture of χSB. For more details see [31].

Acknowledgements. We thank Štefan Olejník and Michael Engelhardt for helpful discussions. This research was supported by the Austrian Science Fund FWF ("Fonds zur Förderung der wissenschaftlichen Forschung") under Contract No. P22270-N16 (R.H.).

References

[1] A. A. Belavin, A. M. Polyakov, A. S. Schwartz, and Y. S. Tyupkin, "Pseudoparticle solutions of the Yang-Mills equations," *Phys. Lett.* **B59**, 85–87 (1975).

[2] A. Actor, "Classical Solutions of SU(2) Yang-Mills Theories," *Rev. Mod. Phys.* **51**, 461 (1979).

[3] G. 't Hooft, "Computation of the quantum effects due to a four- dimensional pseudoparticle," *Phys. Rev.* **D14**, 3432–3450 (1976).

[4] M. F. Atiyah and I. M. Singer, "The Index of elliptic operators. 5", *Annals Math.* **93**, 139–149 (1971).

[5] E.-M. Ilgenfritz and M. Muller-Preussker, "Statistical Mechanics of the Interacting Yang-Mills Instanton Gas", *Nucl. Phys.* **B184**, 443 (1981).

[6] D. Diakonov and V. Y. Petrov, "Chiral Condensate in the Instanton Vacuum," *Phys. Lett.* **B147**, 351–356 (1984).

[7] G. 't Hooft, "On the phase transition towards permanent quark confinement," *Nucl. Phys.* **B138**, 1 (1978).

[8] L. Del Debbio, and M. Faber, and J. Greensite, and Š. Olejník, "Center dominance and Z(2) vortices in SU(2) lattice gauge theory," *Phys. Rev.* **D55**, 2298–2306 (1997).

[9] M. Engelhardt and H. Reinhardt, "Center vortex model for the infrared sector of Yang-Mills theory: Confinement and deconfinement," *Nucl. Phys.* **B585**, 591–613 (2000).

[10] P. de Forcrand and M. D'Elia, "On the relevance of center vortices to QCD," *Phys.Rev.Lett.* **82**, 4582–4585 (1999).

[11] M. Engelhardt, "Center vortex model for the infrared sector of Yang-Mills theory: Quenched Dirac spectrum and chiral condensate," *Nucl.Phys.* **B638**, 81–110 (2002).

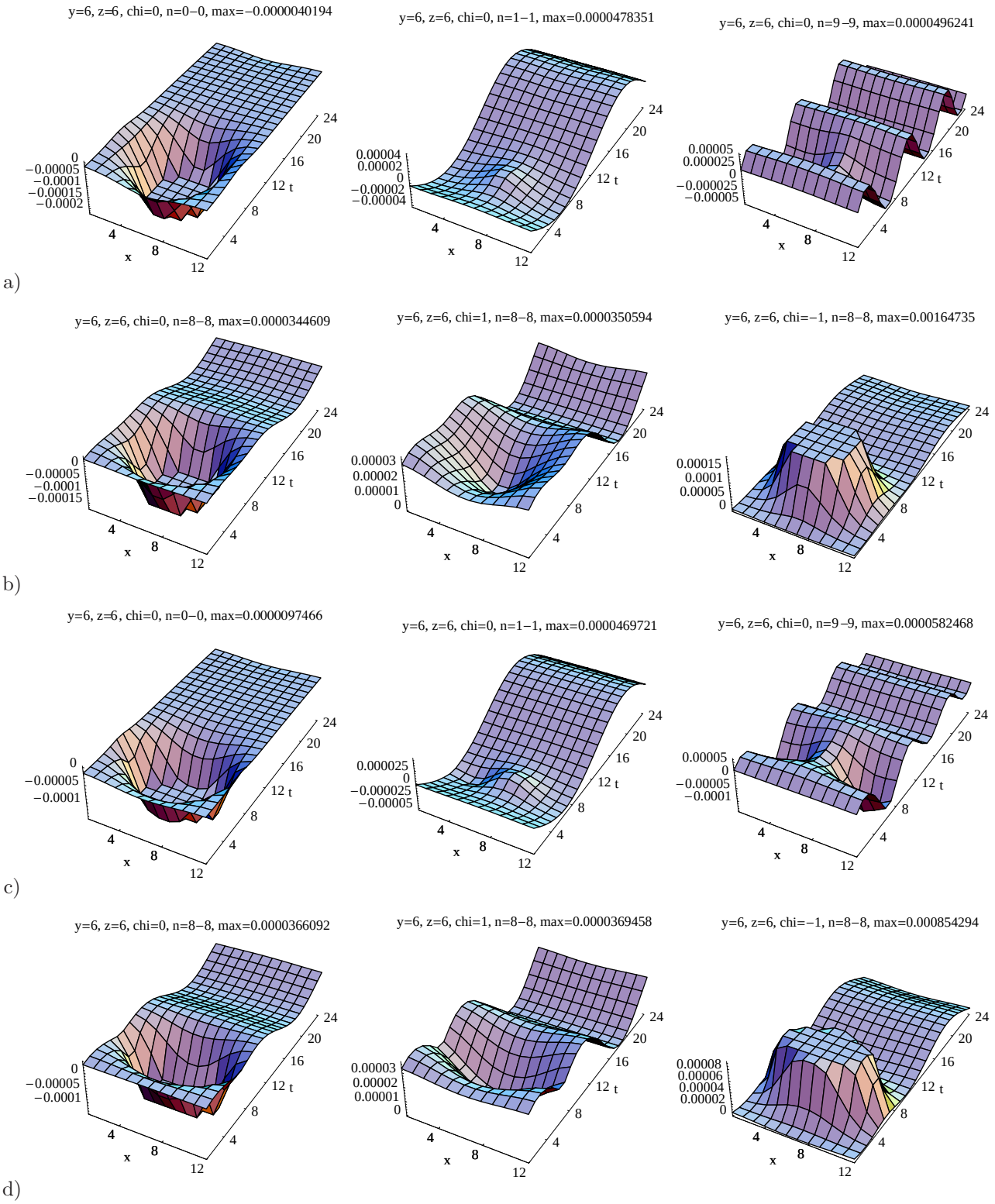

Figure 5. Chiral densities of overlap eigenmodes: a) zero mode (left), first (center), ninth (right) and b) eighth (ρ_5 left, ρ_+ center and ρ_- right) nonzero modes for an instanton; c) and d) the same as a) and b) but for a spherical vortex.

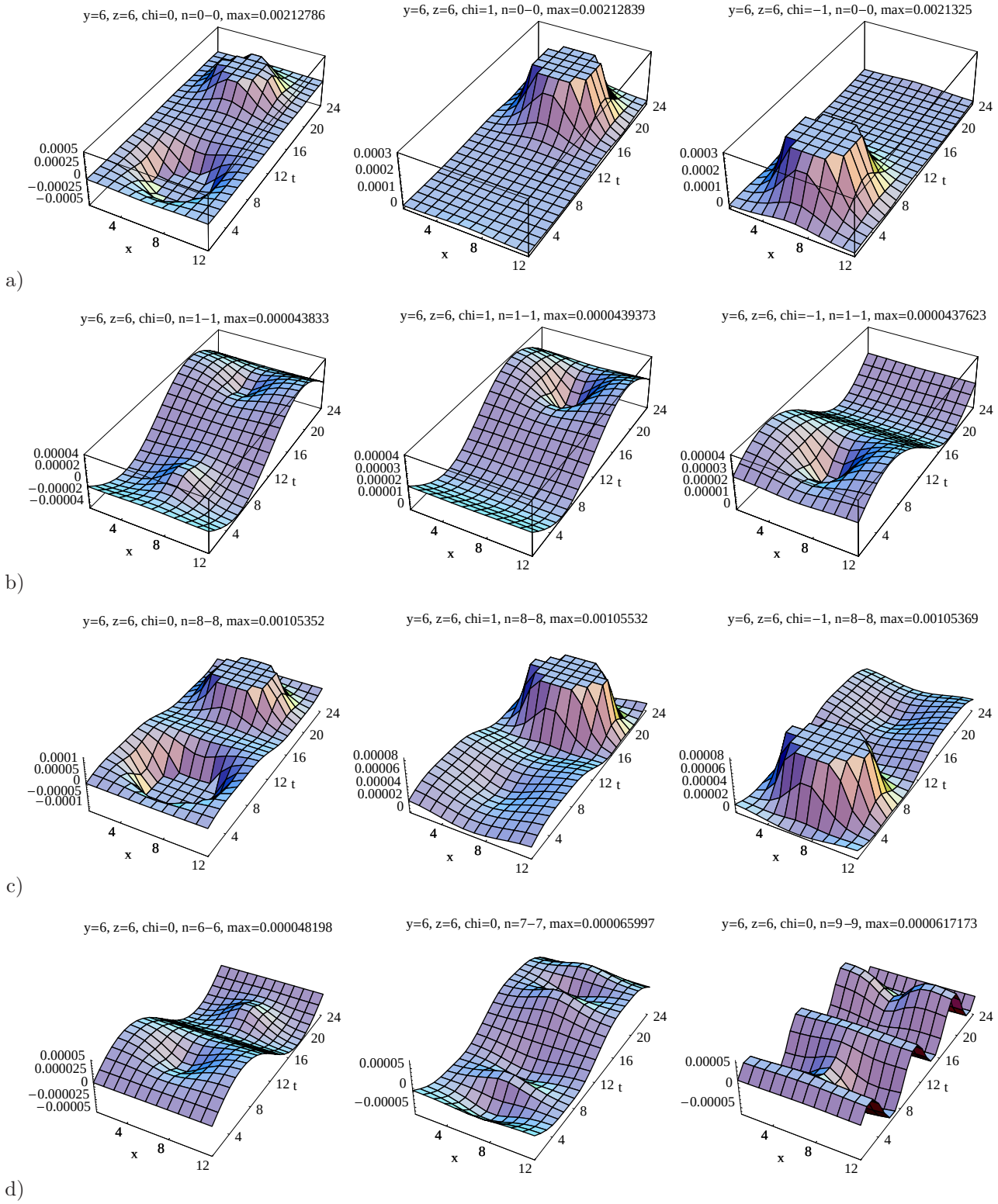

Figure 6. Chiral densities (ρ_5 left, ρ_+ center and ρ_- right column) of the a) lowest (near-zero), b) second-lowest (nonzero) and c) eighth (nonzero) eigenmode of the overlap Dirac operator for an instanton–anti-instanton pair. d) ρ_5 of the sixth (left), seventh (center) and ninth (right) eigenmode.

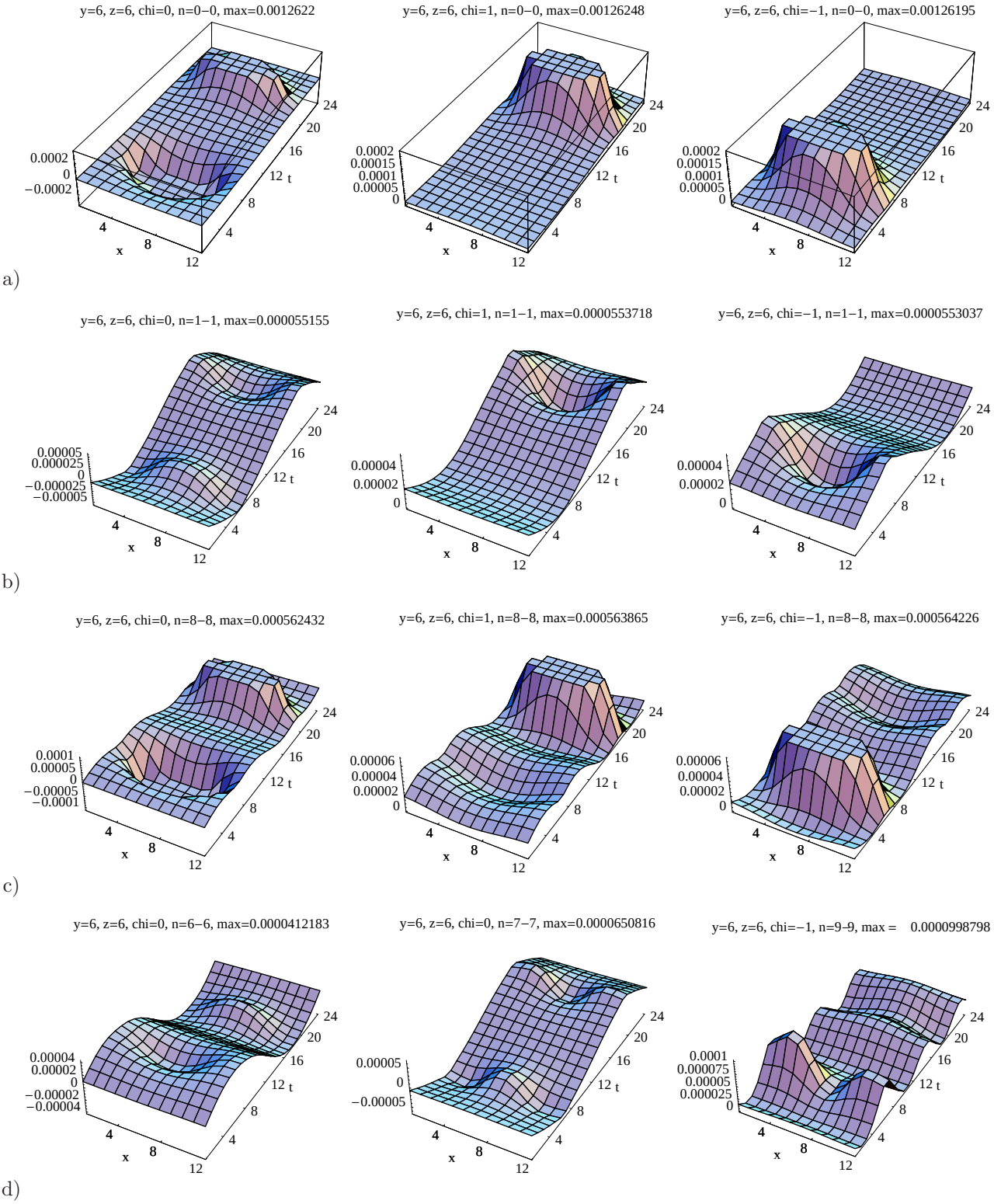

Figure 7. Same as Fig. 6 but for a spherical vortex-anti-vortex pair. Chiral densities (ρ_5 left, ρ_+ center and ρ_- right column) of the a) lowest (near-zero), b) second-lowest (nonzero) and c) eighth (nonzero) eigenmode. d) ρ_5 of the sixth (left), seventh (center) and ninth (right) eigenmode.

[12] R. Höllwieser, and M. Faber, and J. Greensite, and U.M. Heller, and Š. Olejník, "Center Vortices and the Dirac Spectrum," *Phys. Rev.* **D78**, 054508 (2008).

[13] G. Jordan, and R. Höllwieser, and M. Faber, and U.M. Heller, "Tests of the lattice index theorem," *Phys. Rev.* **D77**, 014515 (2008).

[14] T. Banks and A. Casher, "Chiral Symmetry Breaking in Confining Theories," *Nucl. Phys.* **B169**, 103 (1980).

[15] B. Bunk, K. Jansen, B. Jegerlehner, M. Lüscher, H. Simma, *et. al.*, "A New simulation algorithm for lattice QCD with dynamical quarks," *Nucl.Phys.Proc.Suppl.* **42**, 49–55 (1995).

[16] T. Kalkreuter and H. Simma, "An Accelerated conjugate gradient algorithm to compute low lying eigenvalues: A Study for the Dirac operator in SU(2) lattice QCD," *Comput.Phys.Commun.* **93**, 33–47 (1996).

[17] R. Höllwieser, and M. Faber, and U.M. Heller, "Lattice Index Theorem and Fractional Topological Charge, arxiv:1212.3737.

[18] T. Schweigler, R. Höllwieser, M. Faber, and U.M. Heller, "Colorful SU(2) center vortices in the continuum and on the lattice, arxiv:.

[19] M. Engelhardt and H. Reinhardt, "Center projection vortices in continuum Yang-Mills theory," *Nucl. Phys.* **B567**, 249 (2000).

[20] R. Höllwieser, and M. Faber, and U.M. Heller, "Intersections of thick Center Vortices, Dirac Eigenmodes and Fractional Topological Charge in SU(2) Lattice Gauge Theory," *JHEP* **1106**, 052 (2011).

[21] H. Reinhardt and T. Tok, "Merons and instantons in laplacian abelian and center gauges in continuum Yang-Mills theory", *Phys. Lett.* **B505**, 131–140 (2001).

[22] F. Bruckmann, E.-M. Ilgenfritz, B. Martemyanov, and B. Zhang, "The Vortex Structure of SU(2) Calorons," *Phys. Rev.* **D81**, 074501 (2010).

[23] A. Casher, "Chiral Symmetry Breaking in Quark Confining Theories," *Phys. Lett.* **B83**, 395 (1979).

[24] I. Horvath, S. Dong, T. Draper, K. Liu, N. Mathur, *et. al.*, "Uncovering low dimensional topological structure in the QCD vacuum, hep-lat/0212013.

[25] I. Horvath, S. Dong, T. Draper, F. Lee, K. Liu, *et. al.*, "Low dimensional long range topological structure in the QCD vacuum," *Nucl.Phys.Proc.Suppl.* **129**, 677–679 (2004).

[26] P. O. Bowman, K. Langfeld, D. B. Leinweber, A. Sternbeck, L. von Smekal, *et. al.*, "Role of center vortices in chiral symmetry breaking in SU(3) gauge theory," *Phys.Rev.* **D84**, 034501 (2011).

[27] V. Braguta, P. Buividovich, T. Kalaydzhyan, S. Kuznetsov, and M. Polikarpov, "The Chiral Magnetic Effect and chiral symmetry breaking in SU(3) quenched lattice gauge theory," *Phys.Atom.Nucl.* **75**, 488–492 (2012).

[28] E.-A. O'Malley, W. Kamleh, D. Leinweber, and P. Moran, "SU(3) centre vortices underpin confinement and dynamical chiral symmetry breaking," *Phys.Rev.* **D86**, 054503 (2012).

[29] P. Buividovich, T. Kalaydzhyan, and M. Polikarpov, "Fractal dimension of the topological charge density distribution in SU(2) lattice gluodynamics," *Phys.Rev.* **D86**, 074511 (2012).

[30] V. Braguta, P. Buividovich, T. Kalaydzhyan, and M. Polikarpov, "Topological and magnetic properties of the QCD vacuum probed by overlap fermions," *PoS* **ConfinementX**, 085 (2012).

[31] R. Höllwieser, T. Schweigler, M. Faber, and U. M. Heller, "Center Vortices and Chiral Symmetry Breaking in SU(2) Lattice Gauge Theory, arxiv:1304.1277.